11th World Congress on Computational Mechanics (WCCM XI)
5th European Conference on Computational Mechanics (ECCM V)
6th European Conference on Computational Fluid Dynamics (ECFD VI)
E. Oñate, J. Oliver and A. Huerta (Eds)

TOWARDS A MICROMECHANICS-BASED SIMULATION OF CALCANEUS FRACTURE AND FRAGMENTATION DUE TO IMPACT LOADING

Rebecca A. Fielding*, Reuben H. Kraft*

* The Computational Biomechanics Group
Department of Mechanical and Nuclear Engineering
The Pennsylvania State University
341 Leonhard Building
University Park, PA 16802
http://www.mne.psu.edu/compbio/

Key Words: Calcaneus, Finite Element Modeling, Fracture, Microstructure, Simulation

INTRODUCTION

An "underbody blast" (UBB) is the detonation of a mine or improvised explosive device (IED) underneath a vehicle. In recent military conflicts, the incidence of UBBs has led to severe injuries, specifically in the lower extremities [1]. The explosion results in both "local" effects, including inelastic deformations and the rapid acceleration of the vehicle floor following the blast, and "global" effects, which pertain to the gross motion of the vehicle, particularly in the vertical direction [2]. In an idealized scenario, the solider in the vehicle is the 90-90-90 seated position in which the foot and ankle complex, specifically the calcaneus bone, may sustain significant damage [1]. According to information collected regarding blast victims among UK service personnel, 30 individuals presented 40 calcaneal fractures [3]. Despite the importance of calcaneal injuries, this bone's unique properties and the progression of fracture and failure have not been adequately studied under high strain rate loading [4].

It is common when modeling the human body for the trabecular bone to be represented as a homogenous mass within a shell of cortical bone [4][5]. However, this method may be inaccurate. Within a hierarchical modeling framework for biological systems, as shown in Figure 1(a), the components and sub-assemblies are critical to the system-level response. As full system-level human body finite element models become more widely used in the military design process, the need for region-specific constitutive models and robust fracture modeling methods at the component and sub-assembly level will increase. This research discusses early efforts at creating a high-resolution computational model of the calcaneus, with a focus on modeling the complex microstructure of the bone and creating micromechanically-based constitutive models that can be used within full human body models. The ultimate goal is to develop a micromechanics-based simulation of calcaneus fracture and fragmentation due to impact loading. Much of our analysis focused on the length and time scales associated with the dynamic wave propagation without considering the inelastic properties and damage. This is reserved for future and ongoing work.

Figure 1: Range of modeling length scales: (a) high level lower extremity model, (b) calcaneus highlighted within the greater structure, (c) raw microCT image data.

The calcaneus is an irregular bone, comprised mainly of trabecular bone and encased in a thin layer of cortical bone [6][7]. The structural pattern of the calcaneus is developed according to the needs of erect, weight bearing human motion. The major load-bearing column consists of principal compressive trabeculae, which are situated in a path between the posterior articular surface of the talus and the heel. Secondary compression occurs in a trabecular group between the talus and the posterior calcaneal surface. The primary tensile load is carried by trabeculae running between the Achilles tendon towards the front of the bone and the secondary tensile load is borne in the arch of the foot. The area lacking significant trabecular structure is known as the “neutral triangle”. A simplified representation of these structural patterns is shown in Figure 2 [6].

In the general population, the calcaneus is represented in 60% of fractures to the foot and ankle complex [7]. One fracture mechanism occurs due to excessive axial loading in the angle of Gissane, or the angle of the subtalar surface. This generates a fracture line through the neutral triangle with common secondary fracture lines through the upper or posterior surfaces of the bone [6][7]. Intraarticular fractures, representing 75% of adult calcaneal fractures, are commonly classified by the Sanders system. In this system, type I represents non-displaced fractures. Types II-IV refer to the number of articular pieces resulting from the fracture. An A, B, or C following the number further classifies the fracture types. A, B, and C denote whether the fracture line is located laterally, centrally, or medially, respectively. Extraarticular fractures are represented as Type A, B, or C. Type A refers to an anterior fracture, B to a mid-body fracture, and C to a posterior fracture [7].

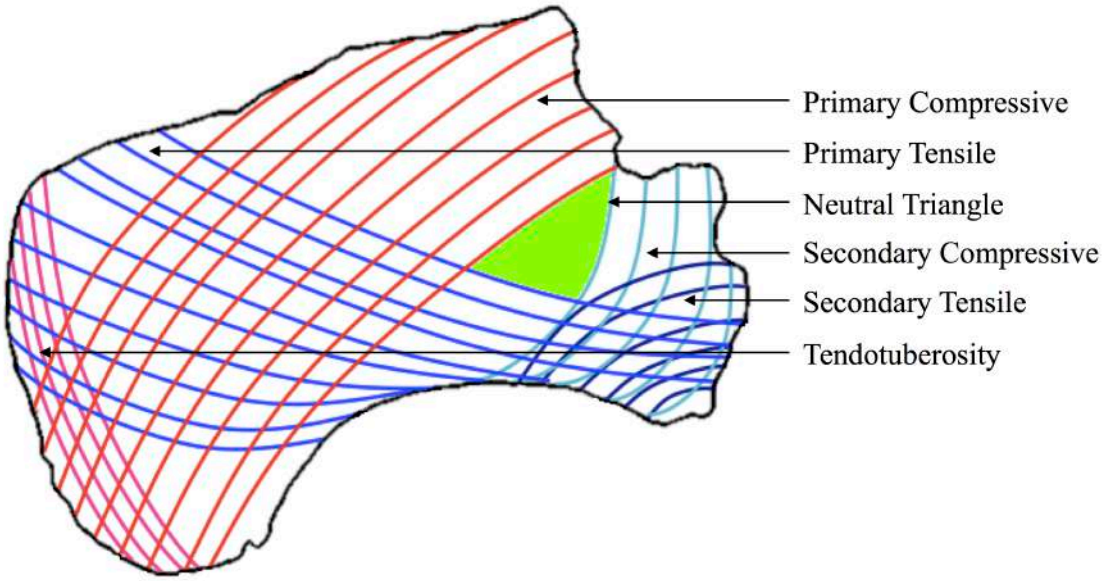

Figure 2: Simplified representation of load bearing trabecular structures in the calcaneus as described by Dhillon [6].

METHODS

Finite element analysis

In using a finite element analysis, dynamic equilibrium is enforced by means of the weak form of the principle of virtual work:

$$\int_{B_0} \boldsymbol{P}: \nabla_0 \boldsymbol{\eta} dV_0 + \int_{B_0} \rho_0 \boldsymbol{b} \cdot \boldsymbol{\eta} dV_0 + \int_{\partial B_0} \bar{\boldsymbol{t}} \cdot \boldsymbol{\eta} dS_0 - \int_{B_0} \rho_0 \boldsymbol{a} \cdot \boldsymbol{\eta} dV_0 = 0 \quad (1)$$

The internal forces in the body are represented by the first term of this equation. External work is represent by the second and third terms. The final term is representative of virtual work In this equation, **P** refers to the first Piola-Kirchoff stress tensor, ∇_0 represents the material gradient, $\boldsymbol{\eta}$ is a virtual displacement which satisfies homogenous boundary conditions over ∂B_0, the : symbol indicates an inner product of second-order tensors, ρ_0 is the density, **b** represents body forces, $\bar{\boldsymbol{t}}$ represents tractions applied to ∂B_0, and **a** refers to acceleration [8].

Anatomic representation

In this effort, a cadaveric calcaneus was scanned to a resolution of 55 μm using an industrial micro-computed tomography (microCT) scanner. The scans were post-processed and used to generate a finite element mesh of the calcaneus. The raw CT data was imported into Avizo Fire [9] and a mid-sagittal plane slice was selected for analysis. A label field was created based on a density threshold of the CT slice to delineate the bone within the slice. It is interesting

to note that cortical shell thickness measurements were taken on both the raw CT slice and the label field. An average thickness of 0.408 mm was found for the cortical shell on the raw slice, (Figure 3a). However, when the measurements were repeated on the label field (Figure 3b), an average thickness of 1.31 mm was found. This discrepancy is attributed to the fineness and complexity of the internal geometry of the bone, especially close to the cortical shell. The detail was difficult to adequately capture when segmenting the bone, and the process should be further refined in future study. A second label field was created to identify the marrow. The label fields were used to generate surfaces for the bone and the marrow, each of which was exported and further processed using Blender in order to create two-dimensional surface meshes, which were converted to spline curves using formZ. Finally, the spline curves (SAT format) were meshed using Trelis (Figure 3c).

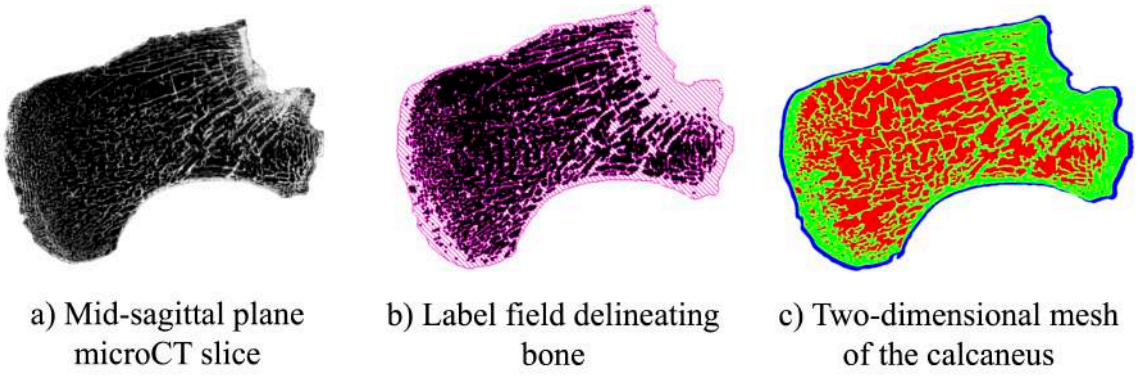

Figure 3: From left to right are shown the three stages of image processing for the calcaneus scan. (a): Unprocessed mid-sagittal CT slice. (b): Label field delineating the bone. (c): The three regions, cortical bone (blue), trabecular bone (green), and marrow (red) that were meshed.

The calcaneus was modeled using two-dimensional quadratic plane strain elements. A fixed boundary condition was applied to the portion of the calcaneus that, in situ, would be restrained by the talus. A displacement of 50 μm was applied to the heel of the calcaneus over 1ms in an explicit dynamic simulation step. The boundary conditions are illustrated in Figure 4. Material properties for the trabecular bone, cortical bone, and bone marrow are given in Table 1 [4][10][11][12]. Currently, the bone is modeled as elastic perfectly plastic. In future studies, more sophisticated fracture modeling techniques will be employed as well as a mesh dependency study to ensure a converged solution. Results of these simulations are described in the following section.

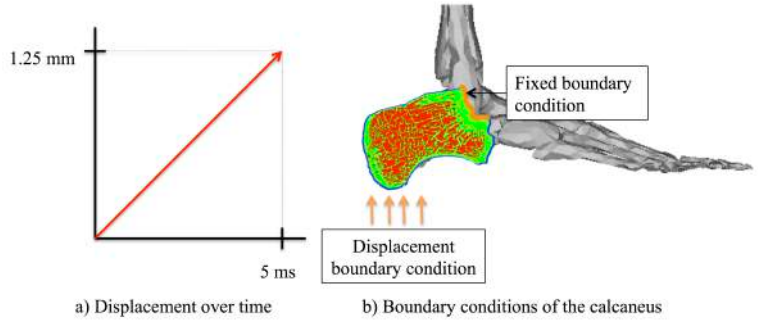

Figure 4: (a) Displacement over time of the heel of the calcaneus. (b) boundary conditions on the calcaneus in Abaqus simulations. There is a displacement of 50 µm impacting the heel over 1ms and a fixed boundary condition representing the talus.

Table 1: Material properties for the biological materials comprising the calcaneus

Material Properties	Cortical Bone	Trabecular Bone	Marrow
ρ (kg/m^3)	1810 [4]	600 [4]	975 [12]
E	15.75 GPa [10]	70 MPa [11]	2 MPa [10]
ν	.325 [10]	.45 [4]	.167 [10]
σ_c (MPa)	132 [4]	1.8 [11]	
K_{IC} (MPa*m$^{1/2}$)	6.4 [10]	.5 [4]	

Plane strain approximation

With the goal of determining the basic mechanisms of fracture propagation through the internal structure of the calcaneus, a two-dimensional model was employed for preliminary simulations. In the absence of rigorous experimental validation, and given the complexity of developing a 3D model of the calcaneus, it was considered a more practical approach to begin with a plane-strain approximation for early investigation. Similar approaches for two-dimensional approximations have been followed elsewhere for the brain [13][14] and the lower extremity [15][16]. As a primary subject of interest is the wave propagation through the calcaneus following dynamic loading, a plane-strain approximation model should provide reasonable preliminary data. However, one important limitation to consider is that, in two dimensions, some of the trabeculae are represented only as islands which, considering marrow as a fluid, may be free to move in the plane, unlike in a three dimensional scenario. This problem may be overcome by the viscous nature of the bone marrow and the time scales associated with the simulation, preventing this nature of motion. Though the fracture pattern may be altered, this approximation will give some indication of dynamic wave propagation.

RESULTS

A typical result for the is shown in Figure 5, which plots the von Mises equivalent stress over the time frame. Following impact, the stress propagates throughout the cortical shell and then begins to radiate into the bone into the bone along the trabeculae. This can be seen in the image as most of the cortical shell has reached a stress of greater than 30 kPa before much of the interior structure has reacted to the impact at all. One can note from the images at .25 ms and .5 ms that the stress seems to travel close to the bottom of the calcaneus along the trabeculae towards the front of the calcaneus prior to spreading towards the top of the calcaneus. It is possible that this pattern of motion may derive from the loading paths illustrated in Figure 2. The stress contours seen in the image raise questions about the interesting and unknown relationship between the bone marrow that fills the pores within the trabecular bone and the way in which stresses are transferred through the trabecular structures. Furthermore, the disappearance and reappearance over time of stress concentrations, for example in the subtalar surface of the calcaneus between .25 ms and .75 ms, may offer insight into the pattern of wave propagation and reflection within the bone.

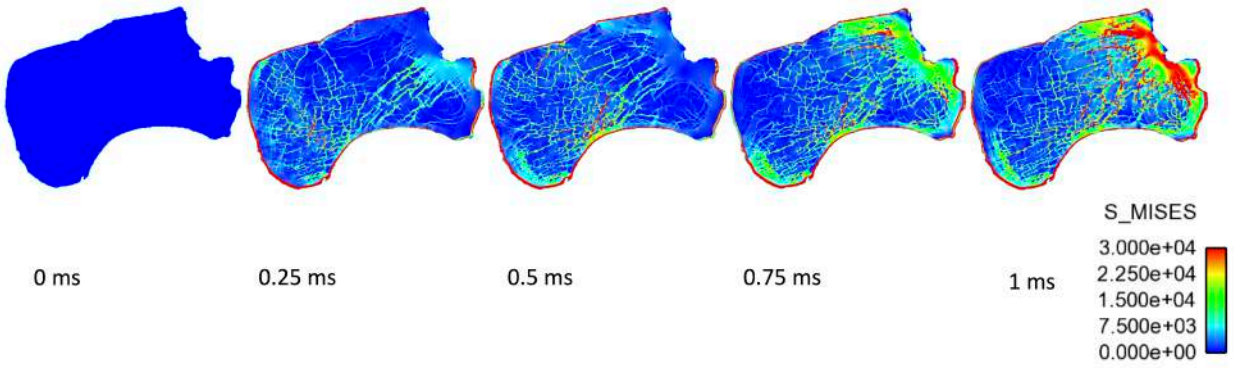

Figure 5: The progression of von Mises stress throughout the calcaneus at .25 ms intervals over the course of the 1 ms simulation.

As can be seen in Figure 6, the cortical bone elements show the highest overall stresses of the three materials, due the higher Young's Modulus of cortical bone. In all three materials, the stress reaches periodic peaks over the timeframe. The marrow elements show much lower stress relative to the other two materials.

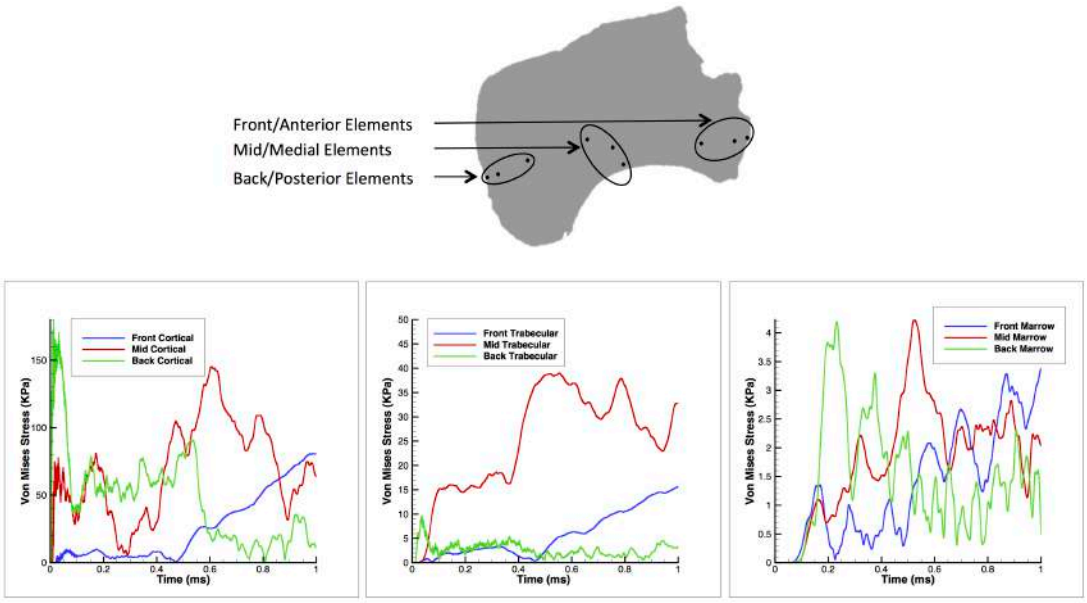

Figure 6: A graph of stress versus time for elements in the front, middle, and back of the calcaneus for cortical bone, trabecular bone, and bone marrow.

DISCUSSION

Examination of the stress patterns over the course of the simulation show local stress concentrations at a variety of points. Figure 7 shows an example of this towards the front of the calcaneus, but additional instances have occurred at other locations in the trabeculae, and generally higher stresses are seen throughout the cortical shell.

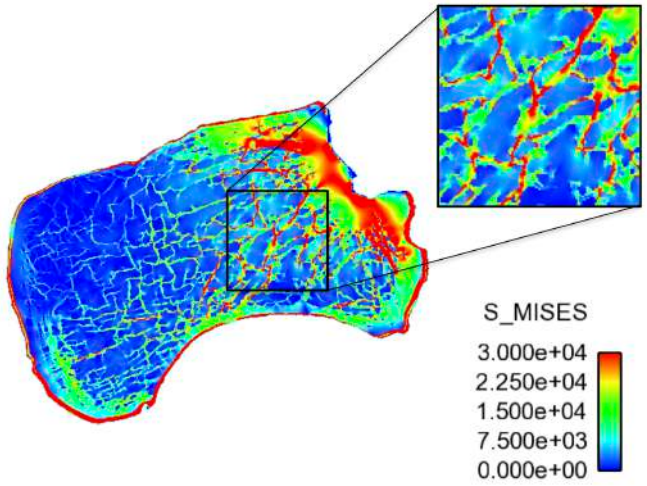

Figure 7: A close up view of local stress concentrations in the calcaneus

The differing material properties between cortical bone and trabecular bone can account for the higher stresses in the cortical shell. However, the reason for the distribution of local stress concentrations in the trabecular structure is less clear. It may be related to the loading paths described in the introduction and illustrated in Figure 2. Another possibility is based on the relative wave speeds in the different materials. Table 2 provides the longitudinal and transverse wave speeds for each material comprising the calcaneus. Additionally, the time necessary for a wave to propagate across the length of the calcaneus (~.0625m) and the height of the calcaneus (~.0376m) is given for each material. These values are averaged for each material to determine the approximate time for a wave to propagate across the whole calcaneus. These values are then averaged to find the approximate wave speed for the model used. As is evident, the wave speeds for the materials composing the calcaneus are very different. A longitudinal wave travels more than 5 times faster in cortical bone than in trabecular bone, and almost 76 times faster than in marrow. Similarly, a transverse wave traveling through cortical bone travels 9 times faster or 61 times faster through cortical bone than through trabecular bone or marrow, respectively. These wave speed discrepancies may contribute to the complexities seen in the stress curves in Figure 6. Interface impedance could also be a contributing factor to the local stress concentrations seen in Figure 7, and will be explored in later studies.

Table 2: Longitudinal and transverse wave speeds in the various materials composing the calcaneus.

	Cortical Bone	**Trabecular Bone**	**Marrow**
Longitudinal Waves			
Longitudinal Wavespeed (m/s)	3559	665.2	46.89
Time across length (s)	1.756E-05	9.395E-05	0.001333
Time across height (s)	1.055E-05	5.646E-05	0.0008011
Average time across (s)	1.406E-05	7.521E-05	0.001067
Average for all materials (s)		0.0003854	
Transverse Waves			
Transverse wavespeed (m/s)	1812	200.6	29.65
Time across length (s)	3.449E-05	0.0003116	0.002108
Time across height (s)	2.073E-05	0.0001873	0.001267
Average Time across (s)	2.761E-05	0.0002494	0.001688
Average for all materials (s)		0.0006549	

In order to better understand the stresses seen, and the effect that the heterogeneity of the calcaneus' composition might have, three simulations were conducted using the same loading conditions, 50μm displacement over 1 ms period of stress propagation, with three different material set ups:

1. Entire calcaneus comprised of cortical bone
2. Calcaneus comprised of a cortical shell with a homogenous trabecular interior
3. Calcaneus comprised of a cortical shell and a trabecular and marrow interior.

Results are illustrated in Figure 8. It is interesting to note the differences in the stress response, especially as evident when the calcaneus is comprised wholly of cortical bone and shows major oscillations rising in stress magnitude throughout. The latter two compositions are mores similar, but differences are evident. The calcaneus with marrow, while showing a peak initial stress similar to that of the calcaneus without marrow, but the stress decreases more quickly, plateaus, then decreases again and remains close to zero for the remainder of the simulation. The calcaneus without marrow, conversely, shows additional stress peaks later in the simulation. A fast Fourier transform was performed for these three curves, as seen in Figure 9. All three scenarios showed amplitude peaks at a high and a low frequency. However, the peak stress amplitude for the low frequency peak is lower with each additional material. For the homogenous composition, this peak amplitude is close to the elastic modulus of cortical bone. The high frequency amplitude peak is much higher for the all cortical bone simulation as well. This value is much lower for the two-material and three-material calcaneus. It is interesting to note, however, that while the low frequency amplitude peak is slightly higher in the two-material calcaneus than the three-material, the high frequency amplitude is slightly lower for this simulation.

Figure 9 shows that in the simulations a wide frequency spectrum is experienced within the calcaneus due to impact loading. Large peaks exist near zero and close to 40000 Hz for the all-cortical case. There are other peaks in the all-cortical case (e.g. at 11, 19, and 39992 Hz) that are currently being examined in more depth since they diminish in the other cases that were considered. These frequency spectra give clues about the important dynamics o the problem and may yield interesting insights when examining failure and inelastic damage in the future.

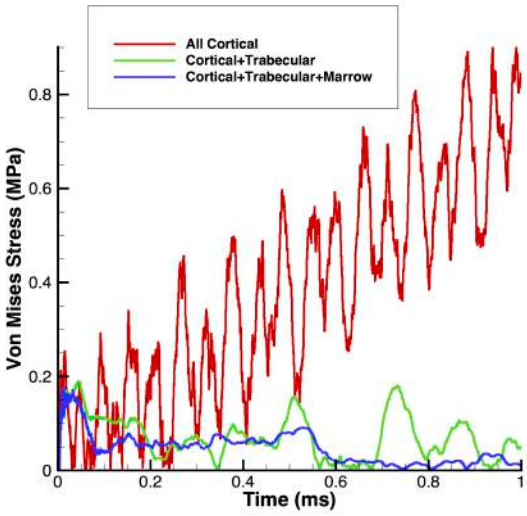

Figure 8: Stress vs Time plots of an element in the back of the calcaneus for three different material compositions.

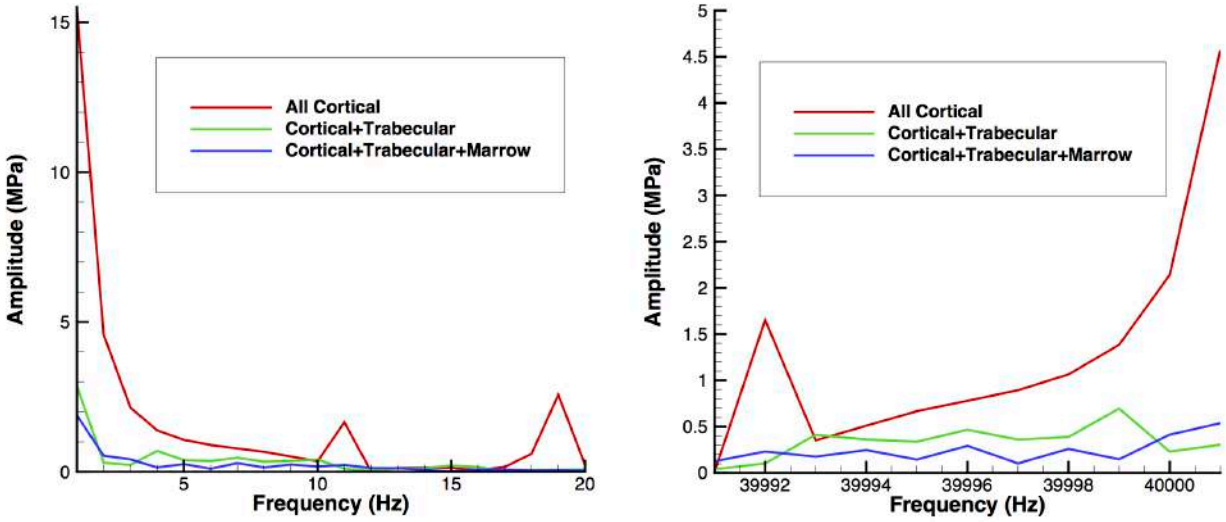

Figure 9: Fast Fourier transforms of stress vs. time curves for three different material compositions of the calcaneus.

CONCLUSION

This paper has presented preliminary study of the dynamic response of the calcaneus bone subjected to impact loading. Our initial results indicate a complex wave propagation problem due to the various materials (cortical bone, trabecular bone, and bone marrow) and their wide range of

mechanical properties. Much of our analysis focused on the length and time scales associated with the dynamic wave propagation without considering the inelastic properties and damage. This is reserved for ongoing and future work.

ACKNOWLEDGEMENTS

This work was supported in part through instrumentation funded by the National Science Foundation through grant OCI–0821527.

REFERENCES

[1] J. Alvarez, "Epidemiology of Blast Injuries in Current Operations," in *A Survey of Blast Injury across the Full Landscape of Military Science*, 2011, p. Keynote KN1.

[2] S. Arepally, D. Gorsich, K. Hope, S. Gentner, and K. Dotleff, "Application of mathematical modeling in potentially survivable blast threats in military vehicles," 2008 [Online]. Available: http://oai.dtic.mil/oai/oai?verb=getRecord&metadataPrefix=html&identifier=ADA496843. [Accessed: 06-Nov-2013]

[3] J. C. Clasper, A. M. J. Bull, A. Ramasamy, I. Gibb, R. Phillip, and A. M. Hill, "The Modern 'Deck-Slap' Injury—Calcaneal Blast Fractures From Vehicle Explosions," *The Journal of Trauma: Injury, Infection, and Critical Care*, vol. 71. pp. 1694–1698, 2011.

[4] R. H. Kraft, M. L. Lynch, and E. W. Vogel III, "Computational Failure Modeling of Lower Extremities." ARL-RP-346, Aberdeen Proving Ground, Maryland, 2012 [Online]. Available: ARL-RP-346

[5] C. Untaroiu, K. Darvish, J. Crandall, B. Deng, and J.-T. Wang, "A finite element model of the lower limb for simulating pedestrian impacts.," *Stapp Car Crash J.*, vol. 49, pp. 157–181, 2005.

[6] M. S. Dhillon, *Fractures of the calcaneus*. New Delhi: Jaypee Brothers, 2013.

[7] K. Badillo, J. A. Pacheco, S. O. Padua, A. A. Gomez, E. Colon, and J. A. Vidal, "Multidetector CT evaluation of calcaneal fractures.," *Radiographics*, vol. 31, pp. 81–92, 2011 [Online]. Available: http://pubs.rsna.org/doi/full/10.1148/rg.311105036

[8] R. H. Kraft, J. F. Molinari, K. T. Ramesh, and D. H. Warner, "Computational micromechanics of dynamic compressive loading of a brittle polycrystalline material using a distribution of grain boundary properties," *J. Mech. Phys. Solids*, vol. 56, no. 8, pp.

2618–2641, Aug. 2008 [Online]. Available: http://linkinghub.elsevier.com/retrieve/pii/S0022509608000549. [Accessed: 31-Jan-2014]

[9] "Avizo User's Guide." Konrad-Zuse-Zentrum fur Informationstechnik Berlin (ZIB), Visualization Sciences Group, SIS, 2013 [Online]. Available: http://www.vsg3d.com/sites/default/files/AvizoUsersGuide.pdf

[10] H. Isaksson, C. C. van Donkelaar, and K. Ito, "Sensitivity of tissue differentiation and bone healing predictions to tissue properties.," *J. Biomech.*, vol. 42, pp. 555–564, 2009.

[11] E. Mittra, C. Rubin, B. Gruber, and Y.-X. Qin, "Evaluation of trabecular mechanical and microstructural properties in human calcaneal bone of advanced age using mechanical testing, microCT, and DXA.," *J. Biomech.*, vol. 41, pp. 368–375, 2008.

[12] U. A. Gurkan and O. Akkus, "The mechanical environment of bone marrow: a review.," *Ann. Biomed. Eng.*, vol. 36, pp. 1978–1991, 2008.

[13] M. B. Panzer, B. S. Myers, B. P. Capehart, and C. R. Bass, "Development of a Finite Element Model for Blast Brain Injury and the Effects of CSF Cavitation," *Annals of Biomedical Engineering*, vol. 40. pp. 1530–1544, 2012.

[14] J. S. Ruan, T. Khalil, and A. I. King, "Human head dynamic response to side impact by finite element modeling.," *J. Biomech. Eng.*, vol. 113, pp. 276–283, 1991.

[15] A. J. Narracott, G. W. John, D. R. Hose, R. J. Morris, J. P. Woodcock, and P. V Lawford, "Influence of intermittent compression cuff design on calf deformation: computational results.," *Conf. Proc. IEEE Eng. Med. Biol. Soc.*, vol. 2007, pp. 6334–6338, 2007.

[16] A. Erdemir, M. L. Viveiros, J. S. Ulbrecht, and P. R. Cavanagh, "An inverse finite-element model of heel-pad indentation," *J. Biomech.*, vol. 39, pp. 1279–1286, 2006.